Nanoscale

Accepted Manuscript

This article can be cited before page numbers have been issued, to do this please use: S. Xiao, B. Skallerud, F. Wang, Z. Zhang and J. He, *Nanoscale*, 2019, DOI: 10.1039/C9NR00104B.

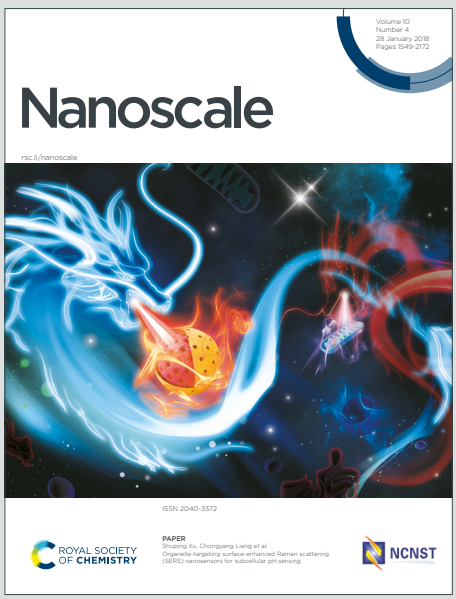

ROYAL SOCIETY OF CHEMISTRY

rsc.li/nanoscale

View Article Online
DOI: 10.1039/C9NR00104B
ROYAL SOCIETY OF CHEMISTRY

Journal Name

ARTICLE TYPE

Cite this: DOI: 10.1039/xxxxxxxxxx

Enabling Sequential Rupture for Lowering Atomistic Ice Adhesion†

Senbo Xiao,*[a] Bjørn Helge Skallerud,[a] Feng Wang,[a] Zhiliang Zhang,[a] and Jianying He*[a]

Received Date
Accepted Date

DOI: 10.1039/xxxxxxxxxx

www.rsc.org/journalname

State-of-the-art passive icephobicity relies mainly on static parameters such as surface energy, coating elastic modulus, crack sizes and so on. Low ice adhesion resulting from dynamic de-icing process, for instance ice detaching modes from substrates, has not yet been explored. In the current study, atomistic modeling and molecular dynamics simulations were employed to identify ice rupture modes as crucial dynamic factors for surface icephobicity. A fish-scale-like icephobic surface prototype enabling low-adhesion sequential rupture of the atomistic interactions at the ice-solid interface was proposed. The novel surface has an intrinsic extended interface rupture pathway, which can lead to a ∼60% reduction in atomistic ice adhesion compared with concurrent ice rupture. This study sheds light on interface mechanical design for surface icephobicity, and could provide solutions for anti-icing, nanoscale tribology and many others. The concept of implementing interfacial rupture modes proposed in this study can also apply to interface design for tailored adhesion mechanics.

Introduction

Excessive icing is hazardous to human activities. From infrastructure to nanodevices, unwanted ice accumulation has posed various challenges in safety and function maintainance[1–4]. Modern strategies for creating passive icephobicity include delaying ice nucleation, superhydrophobicity, and reducing ice adhesion strength by surface engineering and coating design[4–7]. A number of researches have addressed passive icephobic coating, aiming for low ice adhesion strength to enable ice falling off from surfaces by natural factors such as wind or gravity[7–12]. The state-of-the-art passive icephobic coatings have reached ice adhesion strength lower than 1 kPa[13,14].

It is commonly accepted that the ice adhesion strength (τ_c) is governed by the following equation:

$$\tau_c = \sqrt{\frac{E^* G}{\pi a \Lambda}} \quad (1)$$

where E^* is the apparent bulk elastic modulus of the surface, G is the surface energy, a is the crack length, and Λ is a non-dimensional constant determined by the geometric configuration of the crack[15,16]. Formerly reported icephobic coatings, including the famous slippery liquid-infused porous surfaces (SLIPS) and surfaces with embedded multiscale crack initiators[16,17], were designed by manipulating the key parameters in the equation. For instance, lowering elastic moduli and increasing crack length in the coatings were essential options for low ice adhesion and thus icephobicity. It should be noted that the critical crack length of ice adhesion varies on different materials. A recent study assumed the average grain size of ice as the flaw length for calculating ice adhesion strength,[18] the accuracy of which is subjected to further verification.

The governing equation, Eq. 1, relies on static state parameters, and it is thus not surprising that yet one crucial dynamic determinant of ice adhesion strength was not covered, namely the important rupture manner of the interactions between the ice and the surface in the de-icing process. Experiments have demonstrated that atomistic interactions are universally important for ice adhesion strength on different surfaces at the nanoscale[13]. Atomistic interactions at the icing interface underlie ice nucleation, growth and adhesion strength.[19–21] Manipulating the rupture modes of the interfacial atomistic interactions can be an effective way for icephobicity. Study of the dynamic process of de-icing mechanics for low ice adhesion has unfortunately not been investigated to the best of our knowledge.

There are two rupture modes of atomistic interaction at ice adhesion interface, namely the concurrent and sequential modes, as illustrated in Fig. 1. In the concurrent rupture mode, opening the interface requires rupture of all the atomistic interactions at the same time. In this rupture mode, the interface adhesion potential is eliminated in a very short distance, namely a short energy depth

[a] Department of Structural Engineering, The Norwegian University of Science and Technology - NTNU, Trondheim, Norway.
E-mail: senbo.xiao@ntnu.no; jianying.he@ntnu.no

† Electronic Supplementary Information (ESI) available. See DOI: 10.1039/b000000x/

View Article Online
DOI: 10.1039/C9NR00104B

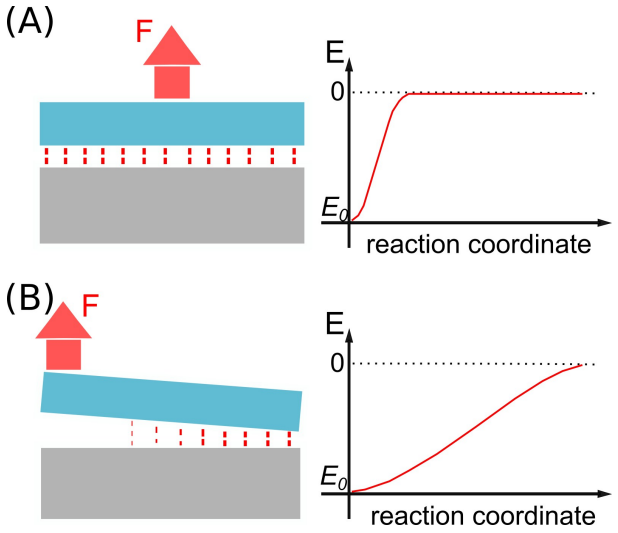

Fig. 1 Two interface rupture modes and their energy profiles. (A) Concurrent and (B) sequential modes with rupture energy profile shown on the right. Atomistic interactions across the interface are indicated as red dashed lines. E_0 denotes the initial adhesive energy state of the interface.

on sub-nanometer atomistic interaction length scale. A short energy depth will result in high rupture force, and thus high stress in de-icing, as depicted schematically in Fig. 1(A). In contrast, in the sequential rupture mode, atomistic interactions are broken in an incremental manner. In this way, the energy depth can be greatly elongated and thus will result in much lower rupture force when compared with the concurrent mode. In anti-icing, and also in many other nanomechanical processes, lower interface rupture force means lower adhesion stress. The difference in mechanics of the two rupture modes is seemingly simple, it is however the basis of formerly observed molecular mechanical functions. These two modes of rupturing atomistic interactions were discovered in molecular mechanics of muscle proteins[22,23]. Specifically, there are two pairs of β-sheets in the same domain structure of the titin kinase, which are designed to be ruptured in the concurrent and sequential modes by evolution, respectively. The pair of β-sheets for sequential rupture was found to always detach first for enabling the mechanochemistry function of the titin kinase[22].

In sequential rupture of atomistic interactions across an interface, it is important to enable opening of the interface in an unzipping manner, as schematically depicted in Fig. 1(B). Thus, it is essential that one end or edge of the interface is flexible while the other end is firmly anchored. The design of a new prototype of icephobic surface with the mechanical function was inspired by the skin of fish. An example of Atlantic salmon fish skin shown in Fig. 2(A). The scales on the fish skin are at one edge firmly linked to the skin, while the other parts are flexible and can be opened to some extent. One can see that for such a tile-like surface setup the ice contact interface is in fact consisting of many smaller interfaces of each single scale, all of which have the potential of unzipping opening as an additional degree of freedom for cracking, thus sequential rupture under pulling stress. Furthermore, the ordered orientation of the scales provide special surface property, that might lead to functions related to surface tribological anisotropy.

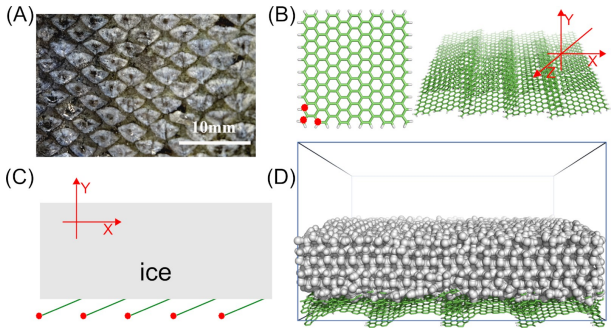

Fig. 2 Featuring scales on fish skin by atomistic modeling. (A) The fish scale structure on Atlantic salmon skin. (B) Graphene platelets used for atomistic modeling. A single platelet with anchor points (red dots) is given on the left. Graphene platelets in pile arranged like fish scales are shown on the right. (C) A schematic of ice on fish-scale-like surface. Graphene platelets and their anchoring points are shown as green line and red dots, respectively. (D) Periodic atomistic system of ice on fish-scale-like surface, with the simulation box shown in blue.

Inspired by this, graphene platelets were used to create fish-scale-like surface at the nanoscale in this study as shown in Fig. 2(B), with focus on theoretical design of a novel icephobic surface prototype. The new icephobic surface has embedded mechanical properties of sequential rupture of atomistic interactions at the ice adhesion interface. De-icing mechanics at two ice rupture modes, concurrent versus sequential, were compared using Molecular Dynamics (MD) simulations. In addition, the effect of low ice adhesion enabled by rupture modes was also compared to the lubricating effect of interfacial water layers. This study proposes for the first time a new mechanical icephobicity for anti-icing research. The concept of interface sequential rupture was also demonstrated by continuum mechanics shedding light on macroscale adhesion mechanics.

Results and discussion

The MD simulations include ice adhesion on the fish-scale-like surface, with and without different thickness of interfacial lubricating water layers, and importantly two ice rupture modes in de-icing mechanics on the surface.

Ice adhesion on fish-scale-like surface

The ice adhered onto the fish-scale-like surface promptly as expected. Because the initial position of the ice was sufficiently close to the surface, the ice swiftly adhered onto the surface in less than 10 ps, leading to a fast decrease in atomistic interaction potential. In the course of 100 ns ice adhesion simulation, the atomistic interactions between the ice and the surface steadily decreased, and finally stabilized, as shown in Fig. 3(B). The adhering face of the ice, the basal face, matched with the topography of the fish-scale-like surface (Suppl.Fig. S1), and deviated from the initial ideal hexagonal ice structure (I_h). This agrees with a former study showing that ice structures formed on a surface have to adapt to the surface morphology and hydrophobicity.[24]. Here, the same effect of the substrate on the ice adhering face is observed,

View Article Online
DOI: 10.1039/C9NR00104B

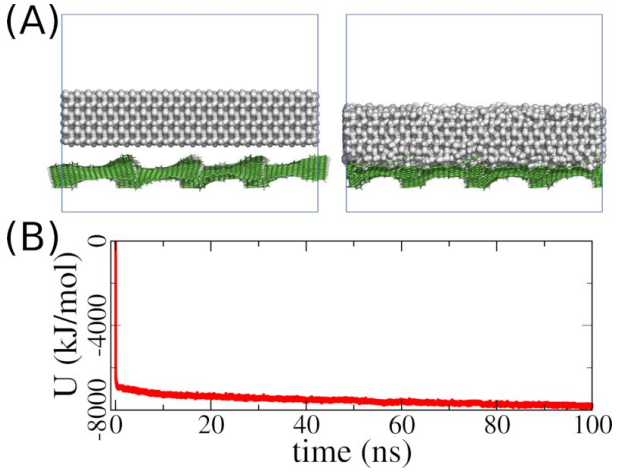

Fig. 3 Ice adhered onto fish-scale-like surface. (A) Snapshots of the system at the beginning (left, $t = 0$ ns) and the end (right, $t = 100$ ns) of the ice adhesion simulation. (B) Atomistic interactions, Lennard-Jones potential (U), between the ice and the surface in the course of 100 ns simulation.

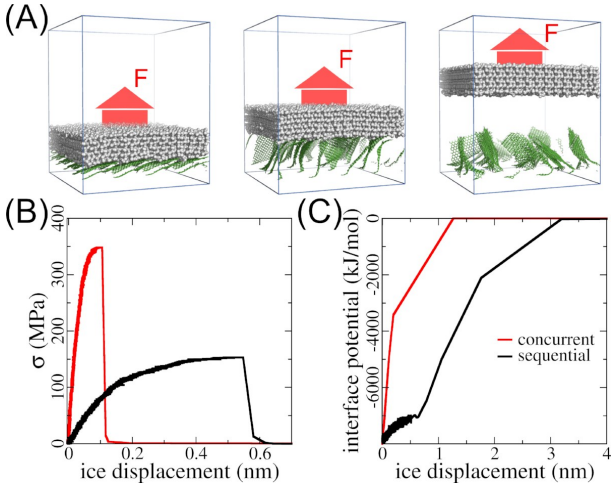

Fig. 4 De-icing on the fish-scale-like surface. (A) Representative snapshots of de-icing process, showing the initial state, sequential rupture of atomistic interactions between graphene platelets and ice, and ice detached from the surface, from the left to the right respectively. Pulling force is indicated in each snapshot. The periodic simulation box was shown in blue. (B) Ice adhering stress profiles observed for the two rupture modes. (C) Interface atomistic interaction potential between ice and the surface monitored for the two rupture modes. (B) and (C) shared the same legends.

namely the substrate geometry determines the topography of the ice adhering face. With the sandwiched lubricating water layer, the ice also adhered onto the surface in the same fast manner, as shown in Suppl.Fig. S2. In all the systems, the atomistic structure of the ice, and the fluidity of the water layer were maintained at the simulation temperature, same to the former report[25]. The final adhered ice onto the fish-scale-like surface, with or without lubricating water layers, had established strong atomistic interactions, which were subjected to mechanical test, namely pulling and shearing, in the following de-icing simulations.

Sequential rupture enabled low ice adhesion

Pulling force was applied to detach the ice from the fish-scale-like surface for comparing the de-icing mechanics of two rupture modes. As shown in Fig. 4(A), the force was acting on the center of mass (COM) of the ice, and was increased linearly with the elongation of the virtual spring moving on the Y-direction of the simulation box. In realizing the sequential rupture mode, each graphene platelet was positionally fixed at their anchoring points as depicted in Fig. 2(B). For the concurrent rupture mode, all the atoms in the whole surface was frozen in the pulling simulations.

Indeed, the sequential rupture mode yielded much lower ice adhesion strength owing to the incremental rupture pattern of the atomistic interactions between the ice and the surface. As example snapshots shown in Fig. 4(A), the graphene platelets were slowly torn from the ice as the ice was lifted by the increasing pulling force. High bending angles of the graphene platelets can be observed at positions close to the ice (Fig. 4(A), middle panel), which signifies distributed traction and thus concentrated stress at these locations on the graphene platelets. Because all the graphene platelets were frozen in the concurrent rupture mode simulations, such a tearing ice phenomenon was not observed, as snapshots shown in Suppl.Fig. S3. From the adhering stress profiles for both rupture modes shown in Fig. 4(B), the rupture stress of ice in the sequential rupture mode showed a ~60% decrease compared to the concurrent mode. The average rupture stress of 5 independent simulations of each rupture mode, σ_r, were 149.75±2.35 MPa and 350.86±3.66 MPa for the sequential and concurrent rupture modes, respectively. The change of the interface potential, namely the sum of the atomistic interactions between the ice and the surface, also varied significantly. As highlighted in Fig. 1, all the atomistic interactions ruptured at the same time in the concurrent rupture mode, which would result in a very short energy depth in the mechanical reaction pathway. The displacement distance of the ice before detaching from the surface can approximate the energy depth in both rupture modes. As can be seen in Suppl.Fig. S4, the concurrent rupture mode showed a very short energy depth of ~0.1 nm. In contrast, the ice was found to have a displacement of ~0.5 nm before its detachment from the surface in the sequential rupture mode, which was 5 times longer than in concurrent mode. The difference in the energy depth of the two rupture modes led to variation of the interface potential between the ice and the surface. As shown in Fig. 4(C), the interface potential increased sharply in the concurrent rupture mode, but showed a much slower increase with fluctuation before rupture event happened in the sequential rupture mode. As indicated by former studies, there are heterogeneous ice structures at the adhesion interface.[24] To further confirm the same results also apply to other faces of I_h, ice with the prism and second prism faces as initial structures for adhering were modeled. As shown in Suppl.Fig. S5, sequential rupture mode leads to much lower adhesion strength than concurrent mode. Thus, the de-icing mechanics of detaching ice from the fish-scale-like surface was in accordance of the mechanical theory shown in Fig. 1, which is efficient in reducing ice adhering stress and is novel to other formerly published surface icephobicity mechanisms.

View Article Online
DOI: 10.1039/C9NR00104B

In the concept of rupture mode enabled lower ice adhesion, a flat surface that fully eliminates sequential rupture can be detrimental to surface icephobicity. To make a strong comparison for the fish-scale-like surface design, additional simulations were carried out with flat graphene as a representative of non-fish-scale-like surface. Despite that the flat graphene surface has similar surface energy as the fish-scale surface, extremely high ice detaching stress was observed on the graphene surface due to absence of sequential rupture (Suppl.Fig. S6).

Shearing ice mechanics

Given that the fish-scale-like surface consisted of graphene platelets with ordered tilting orientation (Fig. 2), anisotropic ice shearing mechanics of ice was expected. As shown in Fig. 5(A), shearing force was applied along and against the graphene platelets tilting direction on the X- and Z-axis of the simulation box. The ice shearing stress profile was similar to formerly reported saw-tooth stick-slip patterns[25–27]. Due to high adhering strength, the ice hopped under shearing force from and re-adhered on the surface sequentially. The highest peaks of the shearing stress were highly uniform when sheared along the graphene platelets tilting orientation, as shown in Fig. 5(B) and Suppl.Fig. S7. In sharp contrast, shearing against the graphene platelets orientation resulted in extraordinarily high stress peaks at the beginning of the shearing simulations, which signified firm interlocking between the ice and the surface (red curves in Fig. 5(B) and Suppl.Fig. S7(B)). Strong interlocking is a sign of heterogeneous ice structures at the ice adhesion interface. The adhesion interface of ice has deviated from the initial structure and into complementing topography with the fish-scale-like surface, which agree with a former study.[24] Such high shearing stress peaks diminished fast in the first half of the simulations, followed by uniform stress peaks similar to shearing along the graphene platelets.

The interlocking effect observed in shearing is caused by the anisotropy of the fish-scale-like surface topography. As can be seen in the Fig. 2(A), the graphene platelets had overlapping areas, which resulted in the roughness of the surface. After the 100 ns adhering simulations, the ice fully covered the surface roughness with ice molecules invaded into the nanoscale grooves at the platelets overlaping edge. As shown in Suppl.Fig. S1, the ice contact interface had a matched roughness pattern to the fish-scale-like surface at the beginning of the shearing. The matched roughness can slide along the graphene platelet tilting direction like walking down a stair-case, but was mechanically locking against the graphene tilting edges. When shearing against the graphene tilting, the mechanical interlocking resulted in high shearing stress in the first half of the shearing simulations. The interlocking of ice and the surface can be in-directly quantified by the contact interface area of the ice. As shown in Fig. 5(C), the ice contact area was almost constant in the whole course of shearing simulation along the graphene tilting direction. When the ice was sheared against the graphene tilting direction, the ice contact interface area demonstrated a sharp increase corresponding to the extraordinary high shearing stress, and steadily

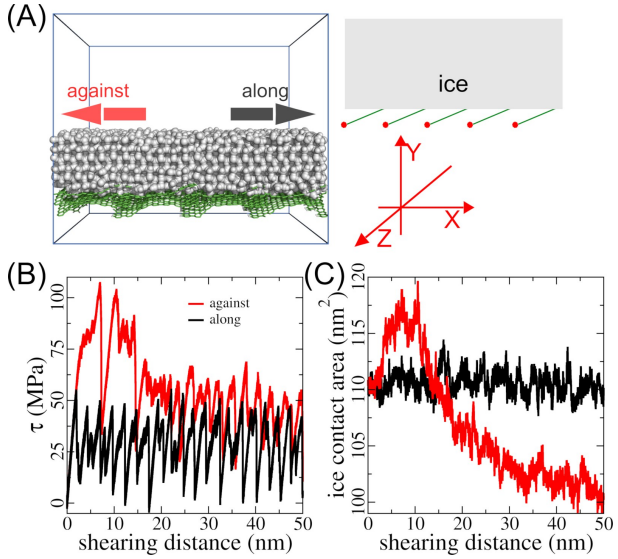

Fig. 5 Shearing ice on the fish-scale-like surface. (A) System snapshot with schematic information of ice shearing directions along and against the tilting orientation of the graphene platelets on the X-axis of the simulation box. The coordinate system of the simulation box is given in the figure. (B) Ice shear stress (τ) profiles observed in the simulations. (C) The contact area of ice at the interface monitored in the same simulation trajectories shown in (B). (B) and (C) shared the same legends.

decrease as the interlocking smoothened out in the second half of the simulation. From snapshots of the ice contact interface topography shown in Suppl.Fig. S1, the increase in ice contact interface area resulted from ice being squeezed in the grooves of graphene platelet overlapping edges under shearing force, which led to enhanced interlocking and thus the high stress peak values. The strong interlocking also led to bending and buckling of some graphene platelets. As shown in Suppl.Fig. S8, distortion of the ordered fish-scale-like graphene platelets can be observed, which led to structural root-mean-squared deviation of the whole substrate. The anisotropic ice shearing mechanics on the fish-scale-like surface could provide surface functions such unidirectional de-icing or water collection, which needs to be further explored.

Lubricating water on fish-scale-like surface

Interfacial lubricating layers of water can result in reduced ice adhesion strength via interfacial slippage, which was confirmed both in experiments and theoretical studies[25,28]. A comparison with nanoscale water layer enabled interfacial slippage can further verify the icephobicity of sequential rupture mode enabled lowering atomistic ice adhesion. Lubricating water layers, with thickness of 1, 2 and 3 nm, were modeled on the fish-scale-like surface as example snapshots shown in Fig. 6(A) and Suppl.Fig. S9. De-icing simulations, detaching and shearing ice with the lubricating water layers, were carried out using the same simulation parameters as above to investigate and compare concurrent and sequential rupture effect on ice adhesion with a lubricating layer medium.

Sequential rupture of atomistic interactions can result in lower ice adhesion strength than the lubricating effect of the interfacial

View Article Online
DOI: 10.1039/C9NR00104B

water layers. Similar to the de-icing without lubricating water, the concurrent and sequential rupture mode were enabled by fixing the whole graphene platelets or the anchoring points, respectively, in the simulations. In concurrent rupture mode, the additional lubricating water layers of all three thicknesses resulted in ∼30% decreased in ice rupture stress as shown in Fig. 6(B, red vs. blue bars), which again confirmed the mechanical effect of the interfacial lubricating water layer in reducing ice adhesion[25]. The sequential rupture of atomistic interactions led to another ∼40% reduction in ice adhesion strength, showing out-performing icephobic effects than the lubricating water layers of all thickness as shown in Fig. 6(B, grey bars). Interestingly, the sequential rupture stress with the lubricating water layer of different thickness were all ∼150 MPa and were close to the value found without the water lubricating layer (Fig. 4(B)), and showed no dependance on the water layer thickness at all. It is important to note that in all the ice detaching simulations, both in concurrent and sequential rupture modes, the water layer and the ice were detached together from the surface despite that the force was only applied on the ice. The interfacial water layer has much stronger atomistic interactions with the ice, importantly hydrogen bonding, than with the fish-scale-like surface. The energy needed for separating ice and water thus was higher than for initiating the openning of graphene platelets and enabling sequential rupture, as the interaction potential shown in Suppl.Fig. S10.

To further test the ice adhesion strength of two rupture modes on ice grown directly on the fish-scale-like surface, the temperature of the interfacial water layer was set to be the same as the ice layer, letting the ice grow for 200 ns. This can reveal possible differences in adhesion strengths in ice attached to the graphene (presented in the previous sections) and when a water layer on graphene evolves into ice. As ice detaching simulation results shown in Suppl.Fig. S11, sequential and concurrent ice rupture stresses were similar the to values above, which again confirmed the low ice adhesion strength by sequential rupture mode. It is noted that the concurrent rupture stress is approximately 10% higher for frozen water layer compared to ice adhesion, whereas in sequential rupture, the frozen water layer gives approximately 10% lower rupture stress when compared to ice adhesion. After deleting the original ice top layer and pulling the newly formed ice only, the same results were observed as shown in Suppl.Fig. S12, showing the sequential rupture mode is constantly outperforming.

The lubricating water layer eliminated the stick-slip pattern in the ice shearing stress, and resulted in much smoother stress profiles. The ice shearing stress profiles showed small fluctuations after the ice started to shear under force, as shown in Fig. 6(C). The ice shear stress was found to depend on the water layer thickness in both shearing along and against the graphene platelet orientation, namely the lower the thickness the higher the shearing stress as shown in Fig. 6(D) and Suppl.Fig. S13. In all systems with different thickness of water layers, higher average stress was observed in shearing against than along the graphene platelet tilting orientation. It is important to note that all the water layers were in a confined space and had a temperature of 255 K. The water molecules in the water layer partially had the properties

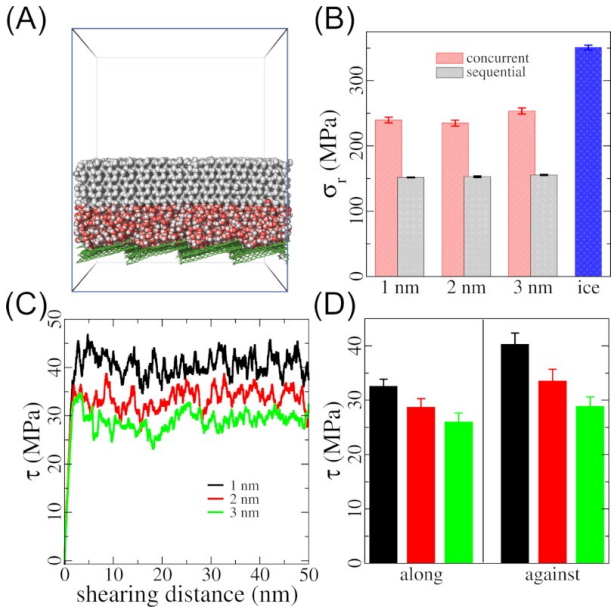

Fig. 6 De-icing mechanics on the fish-scale surface with a lubricating water layer. (A) Representative simulation system snapshot, with a water layer of 2 nm in thickness in a periodic simulation box. (B) Ice adhesion stress (σ) at two rupture modes with different thickness of lubricating water layers. Ice adhesion stress on the fish-scale-like surface without water layer in concurrent rupture mode is shown in blue in the figure for comparison. The error bars show the standard deviation of 5 independent simulations in each dataset. (C) Ice shearing stress (τ) with different thickness of lubricating water layers against the graphene platelet orientation on the X-axis of the simulation box. (D) Average τ observed at the second half of the shearing simulations along and against the graphene platelet orientation on the X-axis of the simulation box, with error bars showing standard deviations. (C) and (D) share the same color code and legends.

of amorphous ice. On the one hand they can quickly fill in the grooves close to the graphene platelets overlapping edges, but on the other hand they featured the interlocking effects shown in Fig. 5.

Conclusion

Practical surface icephobicity is an unsolved problem in research. Former studies have targeted coating and interface properties, such as low elastic moduli, interface slippage and crack initiators, to achieve low ice adhesion strength. Tackling the rupture manner of atomistic interactions between ice and its adhering surface has not been investigated. By comparing the energy changing profiles of two rupture modes shown in Fig. 1, sequential rupture of adhesion indeed outperforms concurrent rupture in term of lower force and thus stress required. By taking inspiration from the ordered orientation of fish scales, the tile arrangement of graphene platelets was able to enable the sequential rupture mode of ice and surface interactions. Given that ice adhesion interfaces are generally not atomistically smooth, macroscale shearing ice on different surface requires both separating atomistic interactions, namely atomistic ice adhesion, and shearing of the interface. The importance of nanoscale detaching and shearing to macroscale adehsion has been identified in former studies.[29]. Both nanoscale detaching and shearing mechanics under-

View Article Online
DOI: 10.1039/C9NR00104B

lie ice adhesion observed in experimental anti-icing shearing test. Atomistic detaching and shearing ice on the fish-scale-like surface were carried out in this study. The results confirmed the effects of sequential rupture modes for low ice adhesion and thus surface icephobicity. This study further compared the sequential rupture mode and the formerly reported lubricating water layer in reducing ice adhesion. The positive theoretical de-icing results need to be verified and applied in future experiments. The icephobic effect of the fish-scale-like surface in this study is a novel approach to surface icephobicity, which is fundamentally different from surfaces with infused oil, lubricating slippage, superhydrophobicity or embedded cracking seeds. The mechanism of the sequential rupture can serve as a new principle for designing new icephobic coatings, and a synergistic option for the already published anti-icing nanotechnology. We note that features of sequential rupturing atomistic interactions were observed in the detachment process of gecko feet from different surfaces.[30,31] Enabling sequential rupture of atomistic interactions for lowering adhesion strength should hold not only on the prototype fish-scale-like surface investigated in this study, but also other surfaces of non-fish-scale-like. The special nanoscale pattern of the fish-scale-like surface could be a first candidate in fabricating icephobic surfaces that enable sequential rupture interface mechanics. Implementing the rupture mode concept in fabricating new icephobic surfaces, including fish-scale-like and non-fish-scale-like, should be addressed in future studies. Similar to the research focusing on gecko feet adhesion mechanics, the fish-scale-like surface prototype could shed light on new bio-inspired icephobic materials. The unzipping manner of sequential rupture for low adhesion strength not only hold at the nanoscale, but in principle should function at the macroscale. Continuum mechanics structural response analysis of adhesion reduction by sequential rupture in tension and shear are provided in the Supplementary Materials. As the ancient Chinese proverb says, it is easy to break one arrow shaft but difficult to break ten at once. The results of this study thus could be a reference for low adhesive surface in general.

Computational Methods

The modeling in this study focused on the design of surface icephobicity in the dynamic de-icing mechanics, namely enabling sequential rupture of atomistic interactions for low ice adhesion strength. The surface prototype in this study featured tiles of graphene platelets arranged in a fish-scale-like pattern. The MD simulations were devoted to test the adhesion strength of ice on the fish-scale-like surface, and additionally with formerly reported interfacial lubricating water layers for comparison.

Atomistic modeling

As shown in Fig. 2(B), the graphene platelets had a uniform size of $\sim 2.3 \times 2.3$ nm^2, and were placed in a periodic tile arrangement on the XZ plane, overlapping one another $\sim$0.6 nm in both the X- and Z-directions. Three carbon atoms at one corner of each graphene platelets are positionally fixed to serve as anchoring points. As such, the graphene platelets had a tilting orientation along the X- and Z-axis, as indicated by Fig. 2(C) and (D). It thus can be expected when ice is lifted in the Y-direction from the fish-scale-like surface, each graphene platelet will be torn from the ice with the atomistic interactions sequentially eliminated as depicted in Fig. 1(B).

Table 1 Atomistic parameters, van der Waals radius (σ) and energy well depth (ε), for the carbon (C) and hydrogen (H) atoms of the graphene platelets.

atom type	σ (nm)	ε (kJ/mol/nm^2)
C	0.355	0.293
H	0.242	0.126

Hexagonal ice (I_h) was used for modeling ice adhesion due to its abundance in the biosphere. As shown in Fig. 2(D), the ice structure is periodic in the X- and Z-direction of the simulation box. Because both the graphene arrangement and the ice structure are periodic in the lateral X- and Z-direction, there is no boundary on the ice adhesion interface, and thus no boundary adhesion effect. The ice had a thickness of $\sim$2 nm, and the same size as the simulation box dimension ($\sim$10.4$\times$10.4 nm^2). The basal face of the ice, (0 0 0 1), was used for contact with the surface. The ice was initially placed close to the surface without any atomistic overlapping, as shown in Fig. 3(A). This enabled fast adhesion of ice in the following simulations for preparing a stable ice adhesion state. Former studies indicated that lubricating quasi-liquid water layers sandwiched at the ice-solid interface significantly reduced ice adhesion strength[25,28]. Such water layers were also modeled for comparison in this study. Interfacial water layers with thickness of 1, 2 and 3 nm were used and placed between the ice and the fish-scale-like surface, resulting in three new systems for ice adhesion strength comparison, as shown in Suppl.Fig. S9.

The atomistic parameters used in this study were consistent with a former study on nanoscale de-icing[25]. The water model tip4p/ice was chosen in modeling the ice[32]. The graphene platelets used bonding, angle and dihedral atomic parameters from OPLS force-field[33,34]. Specifically, the carbon and the hydrogen atoms of the graphene platelets were electrically neutral. The hydrogen atoms with parameters from those in benzene molecules were used to bond with sp2 carbon atoms at the edges of the graphene platelets. The graphene platelets interacted with ice and water via van der Waals forces. Thus, the non-bonded atomistic interactions between the graphene platelets and ice/water molecules decay to a negligible level at a length scale of 1 nm. The detailed atomistic parameters of the graphene platelets are given in Table. 1

Simulations

All the simulations were carried out using the package GROMACS 5.0.7[35]. For all the systems, the Y-axis in all the simulation boxes were more than 2 times larger than the distance from the bottom of fish-scale-surface to the top of the ice, as shown in Fig. 2(D). Such big buffer space of vacuum in the Y-axis of the simulation boxes was used to ensure that the atoms do not interact with their periodic images given by the periodic boundary conditions at any time of the simulations. A cutoff distance of 1.0 nm was cho-

View Article Online
DOI: 10.1039/C9NR00104B

sen for all the nonbonded interactions in all simulation systems. The particle-Ewald method was employed to account for the long-range electrostatic interactions for the water/ice molecules[36], and the LINCS algorithm to constrain bond vibrations was used in order to obtain a larger time step of 0.002 ps[37].

All the atomistic structures in our simulation systems were first subjected to energy minimization utilizing steepest descent algorithm to remove any possible close atom contacts. Subsequently, the ice in all the systems were let to adhere onto the fish-scale-like surface with and without lubricating water layers, and further to reach equilibrated adhesion states. The simulations were carried out in the NVT ensemble at varied temperature for different components of the simulation systems. The Nosé-Hoover coupling method was used to maintain the temperature of the simulation systems[38,39], with a coupling time constant $\tau_T = 0.4$ ps. The temperature of the ice was kept at 180 K, as formerly confirmed that the ice structure by tip4p/ice was stable at this temperature[25]. The lubricating water layers were kept at 255 K, and the fish-scale-like graphene platelets was kept at 180 K. All the systems were equilibrated for 100 ns, during which the ice adhesion to the surface occurred. The final equilibrated structures, i.e. ice adhered on the fish-scale-like surface, were used for force-probe MD simulations of pulling and shearing.

The ice in all the simulation systems was subjected to pulling force in force-probe MD simulations to access the adhesion strength on the fish-scale-like surface, with and without different thickness of interfacial water layers[40]. Specifically, the center of the mass (COM) of the ice was linked to a moving virtual harmonic spring with a spring constant of 500 kJ/mol/nm^2. The spring was initially placed at the COM of the ice and was set to move at a constant speed of 0.5 nm/ns vertically from the surface for ice detaching, as shown in Fig. 4(A). For shearing the ice on the surface, the spring was pulled horizontally along and against the graphene tilting directions, as shown in Fig. 5(A). Because of the periodic boundary conditions, there is no buffering space for accommodating the moving spring in the shearing simulations. In order to generate sufficient force for ice shearing, a higher spring constant of 2000 kJ/mol/nm^2 was used. It should be noted that the pulling force was applied on the ice only, and neither on the fish-scale-like surface nor the interfacial water layers. The simulation trajectories and the pulling force generated by the displacement between the spring and the ice were collected every 5 ps for calculating the ice adhering and shearing stresses. The ice adhering stress, σ, was monitored via normalizing the observed pulling force ($F_{pulling}$) by the ice-substrate contact area (A), as shown by Eq. 2. The rupture stress, σ_r, was the highest ice adhering stress collected during pulling. Five independent simulations were performed for detaching ice from the fish-scale-like surface with and without interfacial water layers of different thickness each. Likewise, the shearing stress, τ, was obtained by normalizing the shearing force ($F_{shearing}$) by the ice contact area A, as shown in Eq. 3.

$$\sigma = \frac{F_{pulling}}{A} \quad (2)$$

$$\tau = \frac{F_{shearing}}{A} \quad (3)$$

It is important to note the absolute stress values obtained in the simulations are loading rate dependent, which are confirmed by former studies utilizing the same simulation protocols.[25,41] The difference in adhesion stress of two rupture modes observed under the same loading rate is yet significant.

Conflicts of interest

There are no conflicts to declare.

Acknowledgements

The authors thank the support from the Research Council of Norway through the FRINATEK project Towards Design of Super-Low Ice Adhesion Surfaces (SLICE, 250990). The computational resources were provided by Norwegian Metacenter for Computational Science (NOTUR NN9110k and NN9391k).

Notes and references

1 R. Carriveau, A. Edrisy, P. Cadieux and R. Mailloux, *Journal of Adhesion Science and Technology*, 2012, **26**, 447–461.
2 F. Caliskan and C. Hajiyev, *Progress in Aerospace Sciences*, 2013, **60**, 12–34.
3 F. Cucchiella and I. D'Adamo, *Renewable and Sustainable Energy Reviews*, 2012, **16**, 5245–5259.
4 M. J. Kreder, J. Alvarenga, P. Kim and J. Aizenberg, *Nature Reviews Materials*, 2016, **1**, 15003.
5 V. Hejazi, K. Sobolev and M. Nosonovsky, *Scientific reports*, 2013, **3**, 2194.
6 Z. He, E. T. Vågenes, C. Delabahan, J. He and Z. Zhang, *Scientific reports*, 2017, **7**, 42181.
7 F. Wang, W. Ding, J. He and Z. Zhang, *Chemical Engineering Journal*, 2019, **360**, 243–249.
8 H. Sojoudi, M. Wang, N. Boscher, G. McKinley and K. Gleason, *Soft matter*, 2016, **12**, 1938–1963.
9 K. Golovin, S. P. Kobaku, D. H. Lee, E. T. DiLoreto, J. M. Mabry and A. Tuteja, *Science Advances*, 2016, **2**, e1501496.
10 E. J. Y. Ling, V. Uong, J.-S. Renault-Crispo, A.-M. Kietzig and P. Servio, *ACS applied materials & interfaces*, 2016, **8**, 8789–8800.
11 S. Bengaluru Subramanyam, V. Kondrashov, J. Rühe and K. K. Varanasi, *ACS applied materials & interfaces*, 2016, **8**, 12583–12587.
12 Y. Zhuo, V. Håkonsen, Z. He, S. Xiao, J. He and Z. Zhang, *ACS applied materials & interfaces*, 2018, **10**, 11972–11978.
13 Z. He, Y. Zhuo, J. He and Z. Zhang, *Soft matter*, 2018, **14**, 4846–4851.
14 C. Urata, G. J. Dunderdale, M. W. England and A. Hozumi, *Journal of Materials Chemistry A*, 2015, **3**, 12626–12630.
15 M. Nosonovsky and V. Hejazi, *ACS nano*, 2012, **6**, 8488–8491.
16 Z. He, S. Xiao, H. Gao, J. He and Z. Zhang, *Soft matter*, 2017, **13**, 6562–6568.
17 P. Kim, T.-S. Wong, J. Alvarenga, M. J. Kreder, W. E. Adorno-Martinez and J. Aizenberg, *ACS nano*, 2012, **6**, 6569–6577.

View Article Online
DOI: 10.1039/C9NR00104B

18 M. Pervier, B. G. Lerma, E. P. Moncholi and D. Hammond, *Engineering Fracture Mechanics*, 2019, DOI:10.1016/j.engfracmech.2019.01.039.

19 J. Liu, C. Zhu, K. Liu, Y. Jiang, Y. Song, J. S. Francisco, X. C. Zeng and J. Wang, *Proceedings of the National Academy of Sciences*, 2017, **114**, 11285–11290.

20 Z. He, K. Liu and J. Wang, *Accounts of chemical research*, 2018, **51**, 1082–1091.

21 F. Wang, S. Xiao, Y. Zhuo, W. Ding, J. He and Z. Zhang, *Mater. Horiz.*, 2019, DOI:10.1039/C9MH00859D.

22 F. Gräter, J. Shen, H. Jiang, M. Gautel and H. Grubmüller, *Biophysical journal*, 2005, **88**, 790–804.

23 S. Xiao and F. Gräter, *Biophysical journal*, 2014, **107**, 965–973.

24 M. Fitzner, G. C. Sosso, S. J. Cox and A. Michaelides, *Journal of the American Chemical Society*, 2015, **137**, 13658–13669.

25 S. Xiao, J. He and Z. Zhang, *Nanoscale*, 2016, **8**, 14625–14632.

26 J. R. Blackford, G. Skouvaklis, M. Purser and V. Koutsos, *Faraday discussions*, 2012, **156**, 243–254.

27 M. Beeman, W. Durham and S. Kirby, *Journal of Geophysical Research: Solid Earth*, 1988, **93**, 7625–7633.

28 J. Chen, Z. Luo, Q. Fan, J. Lv and J. Wang, *Small*, 2014, **10**, 4693–4699.

29 B.-m. Z. Newby, M. K. Chaudhury and H. R. Brown, *Science*, 1995, **269**, 1407–1409.

30 K. Autumn, Y. A. Liang, S. T. Hsieh, W. Zesch, W. P. Chan, T. W. Kenny, R. Fearing and R. J. Full, *Nature*, 2000, **405**, 681.

31 Y. Tian, N. Pesika, H. Zeng, K. Rosenberg, B. Zhao, P. McGuiggan, K. Autumn and J. Israelachvili, *Proceedings of the National Academy of Sciences*, 2006, **103**, 19320–19325.

32 J. Abascal, E. Sanz, R. García Fernández and C. Vega, *The Journal of chemical physics*, 2005, **122**, 234511.

33 W. L. Jorgensen and J. Tirado-Rives, *Journal of the American Chemical Society*, 1988, **110**, 1657–1666.

34 W. L. Jorgensen, D. S. Maxwell and J. Tirado-Rives, *Journal of the American Chemical Society*, 1996, **118**, 11225–11236.

35 M. J. Abraham, T. Murtola, R. Schulz, S. Páll, J. C. Smith, B. Hess and E. Lindahl, *SoftwareX*, 2015, **1**, 19–25.

36 T. Darden, D. York and L. Pedersen, *The Journal of chemical physics*, 1993, **98**, 10089–10092.

37 B. Hess, H. Bekker, H. J. Berendsen and J. G. Fraaije, *Journal of computational chemistry*, 1997, **18**, 1463–1472.

38 S. Nosé, *The Journal of chemical physics*, 1984, **81**, 511–519.

39 W. G. Hoover, *Physical review A*, 1985, **31**, 1695.

40 H. Grubmüller, B. Heymann and P. Tavan, *Science*, 1996, **271**, 997–999.

41 S. Xiao, Z. Zhang and J. He, *Physical Chemistry Chemical Physics*, 2018, **20**, 24759–24767.

View Article Online
DOI: 10.1039/C9NR00104B

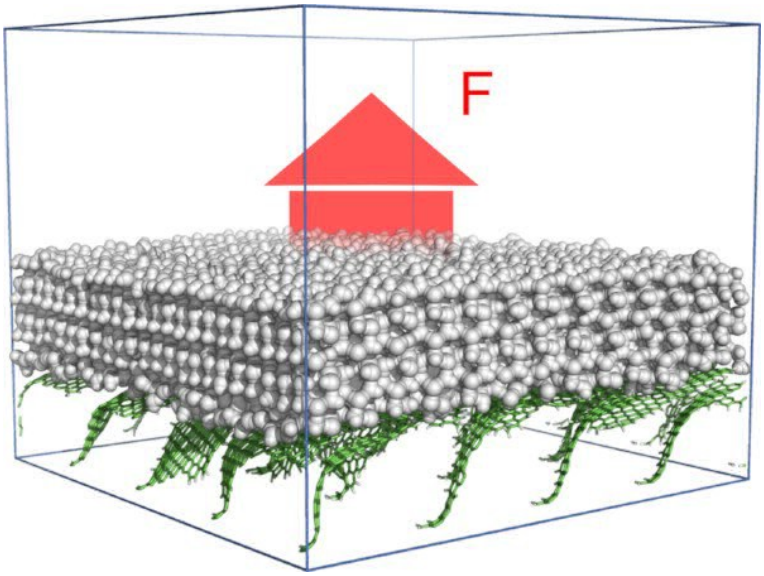

Embedding intrinsic sequential rupture mode into surfaces as interfacial mechanical function can lead to low atomistic ice adhesion strength.